Supporting Information for

Insights into the Excited State Dynamics of Fe(II) Polypyridyl Complexes from

Variable-Temperature Ultrafast Spectroscopy

Monica C. Carey,[a] Sara L. Adelman,[b] James K. McCusker[c]*

Contribution from the Department of Chemistry, Michigan State University

578 South Shaw Lane, East Lansing, MI 48824

[a]*Email address: careymon@chemistry.msu.edu*

[b]*Email address: adelman7@chemistry.msu.edu*

[c]*Email address: jkm@chemistry.msu.edu*

Table of Contents

List of Figures and Tables

Experimental

Characterization of the free ligands and Fe(II) complexes. 2,2'-bipyridine (bpy) ^{1}H NMR (500 MHz, [d$_6$-acetone], δ) [8.67 (ddd, 1 H, J = 0.82, 2.73, 4.65 Hz), 8.48 (dt, 1 H, J = 1.08, 7.96 Hz), 7.92 (ddd, 1 H, J = 1.8, 7.64 Hz), 7.41 (ddd, 1 H, 1.23, 2.72, 6.1 Hz)].

4,4'-dimethyl-2,2'-bipyridine (dmb) ^{1}H NMR (500 MHz, [d$_6$-acetone], δ) [8.51 (d, 1 H, J = 4.72 Hz), 8.30 (m, 1 H), 7.23 (m, 1 H), 2.44 (s, 3 H)].

4,4'-di-*tert*-butyl-2,2'-bipyridine (dtbb) ^{1}H NMR (500 MHz, [d$_6$-acetone], δ) [8.58 (dd, 1 H, J = 0.77, 5.23 Hz), 8.54 (dd, 1 H, J = 0.75, 2.0 Hz), 7.44 (dd, 1 H, J = 2.03, 5.14 Hz)].

Tris(2,2'-bipyridine) iron(II) hexafluorophosphate [Fe(bpy)$_3$](PF$_6$)$_2$ ^{1}H NMR (500 MHz, [d$_6$-acetone], δ) [8.85 (d, 1 H, J = 8.09 Hz), 8.27 (t, 1 H, J = 7.84 Hz), 7.74 (d, 1 H, J = 5.61 Hz), 7.59 (t, 1 H, J = 6.79 Hz)]. ESI-MS (m/z): [C$_{30}$H$_{24}$N$_6$Fe]$^{2+}$ calcd. 262.07; found 262.06.

Tris(4,4'-dimethyl-2,2'-bipyridine) iron(II) hexafluorophosphate [Fe(dmb)$_3$](PF$_6$)$_2$ ^{1}H NMR (500 MHz, [d$_6$-acetone], δ) [8.70 (s, 1 H), 7.51 (d, 1 H, J = 5.79), 7.40 (dd, 1 H, J = 1.23, 5.82), 2.58 (s, 3 H)]. ESI-MS (m/z): [C$_{36}$H$_{36}$N$_6$Fe]$^{2+}$ calcd. 304.12; found 304.10.

Tris(4,4'-di-*tert*-butyl-2,2'-bipyridine) iron(II) hexafluorophosphate [Fe(dtbb)$_3$](PF$_6$)$_2$ ^{1}H NMR (500 MHz, [d$_6$-acetone], δ) [8.94 (d, 1 H, J = 1.75 Hz), 7.57 (d, 1 H, J = 5.69 Hz), 7.52 (d, 1 H, J = 5.93 Hz), 1.40 (s, 9 H). ESI-MS (m/z): [C$_{36}$H$_{36}$N$_6$Fe]$^{2+}$ calcd. 430.26; found 430.28.

Bis(2,2':6',2"-terpyridine) iron(II) hexafluorophosphate [Fe(terpy)$_2$](PF$_6$)$_2$ ^{1}H NMR (500 MHz, [d$_6$-acetone], δ) [9.25 (d, 2 H, J = 8.06 Hz), 8.88 (t, 1 H, J = 7.99 Hz), 8.80 (ddd, 2 H, J = 0.6, 2.11, 8.07 Hz), 8.05 (td, 2 H, J = 1.48, 7.72 Hz), 7.44 (ddd, 2 H, J = 0.6, 2.3, 5.74 Hz), 7.25 (ddd, 2 H, J = 0.6, 1.32, 6.54 Hz). ESI-MS (m/z): [C$_{30}$H$_{22}$N$_6$Fe]$^{2+}$ calcd. 261.06; found 261.04.

Growth of single crystals. [Fe(dmb)$_3$](PF$_6$)$_2$ was recrystallized by vapor diffusion of diethyl ether into methanol, while [Fe(terpy)$_2$](PF$_6$)$_2$ was recrystallized by vapor diffusion of

4

diethyl ether into acetonitrile. In both cases, the single crystals were mounted in paratone oil and transferred to the cold nitrogen gas stream of the diffractometer for data collection.

Crystal structure determination. $[Fe(dmb)_3](PF_6)_2$ crystal data: $C_{40}H_{45}F_{12}FeN_6OP_2$, $M_r = 971.61$, triclinic, a = 8.6648(2) Å, b = 14.3856(3) Å, c = 17.4683(4) Å, T= 173 K, space group P-1 (No. 2), Z = 2, 25863 reflections measured, 7808 unique (Rint = 0.1207), which were used in all calculations. The final wR(F2) was 0.0625 (all data). CCDC 1810752.

$[Fe(terpy)_2](PF_6)_2$ crystal data: $C_{34}H_{28}F_{12}FeN_8P_2$, $M_r = 894.43$, tetragonal, a = 12.3462(2) Å, b = 12.3462(2) Å, c = 48.9067(9) Å, T = 173 K, space group $P4_1$ (no. 76), Z = 8, 26729 reflections measured, 11934 unique (Rint = 0.0446), which were used in all calculations. The final wR(F2) was 0.1140 (all data). CCDC 1810753.

Ground state absorption spectra. The same pump probe cross-section was used to study each of the complexes. Specifically, all four compounds were excited at 490 nm and probing at 530 nm. An overlay of the ground state absorption spectra for the four complexes can be seen in Fig. S1. The spectra have been normalized to the excitation energy for an absorbance of 0.7, as is used for these experiments. All three of the $[Fe(bpy')_3]^{2+}$ complexes have very similar spectra, with the typical MLCT band shape centered around ca. 500 nm. In the case of $[Fe(bpy)_3]^{2+}$, the manifold is narrower, with the red edge being blue-shifted relative to the other two complexes. At the probe wavelength, the absorbance for $[Fe(bpy)_3]^{2+}$ is 0.74 AU, and is 0.8 for $[Fe(dmb)_3]^{2+}$ and $[Fe(dtbb)_3]^{2+}$. $[Fe(terpy)_2]^{2+}$, however, is another case, entirely. The entire MLCT manifold is red-shifted compared to the bpy-based family. It also displays much sharper features. Because of these factors, the absorbance at the probe wavelength is 1.0 AU. For all of these complexes, the rather high absorption at the probe energy serves to decrease the detected signal by way of reducing the amount of light transmitted through the sample. All kinetics were checked for

linearity, however, and signal was optimized by focusing the pump and probe as tightly as possible within the sample.
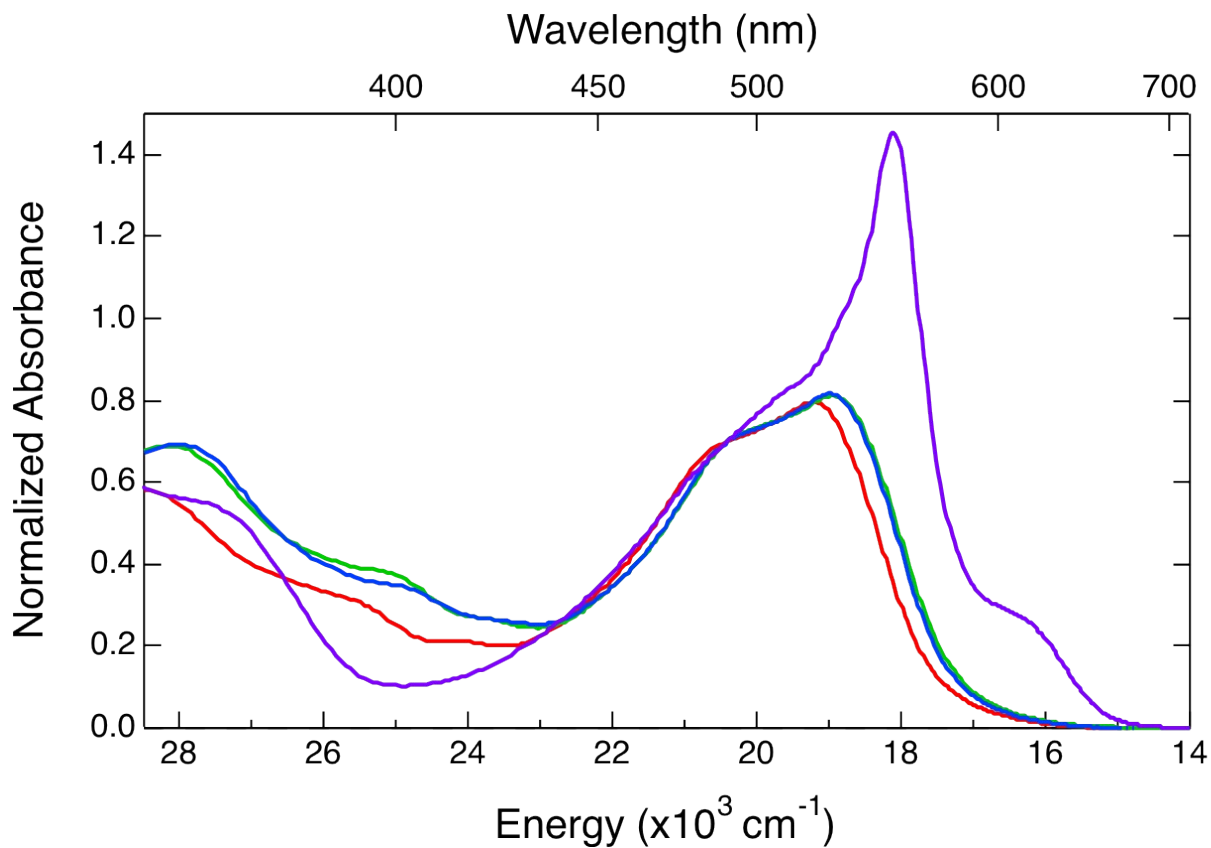
Figure S1.   *Ground state absorption spectra of the four Fe(II) polypyridyl complexes: [Fe(bpy)₃](PF₆)₂ in red, [Fe(dmb)₃](PF₆)₂ in green, [Fe(dtbb)₃](PF₆)₂ in blue, and [Fe(terpy)₂](PF₆)₂ in purple. All spectra are normalized to 0.7 AU at 490 nm (~20400 cm⁻¹). See text for details.*

*Electrochemical data.*

Table S1. Electrochemical data for [Fe(bpy')$_3$]$^{2+}$ series and [Fe(terpy)$_2$]$^{2+}$.

Complex	$E_{1/2}^{ox}$ (V)	ΔE_p (mV)	$E_{1/2}^{red}$ (V)	ΔE_p (mV)	ΔE_p(Fc/Fc$^+$) (mV)
[Fe(bpy)$_3$](PF$_6$)$_2$	0.68	67	-1.74	52	65
[Fe(dmb)$_3$](PF$_6$)$_2$	0.52	62	-1.84	64	62
[Fe(dtbb)$_3$](PF$_6$)$_2$	0.53	59	-1.83	70	61
[Fe(terpy)$_2$](PF$_6$)$_2$	0.72	65	-1.64	63	60

Results and Discussion

Water content of acetonitrile. Fe(II) polypyridyl complexes are known to show a solvent dependence on ground state recovery rate.[1] Additionally, relative to acetonitrile (228 K), the solvent used in these studies, water has a significantly higher freezing point at 273 K. The presence of water, then, in the solvent in large enough quantities could serve to affect the observed rates, and therefore all subsequently calculated parameters. To prevent against this, HPLC grade acetonitrile was chosen, and the water content was measured by ^{1}H NMR (Fig. S2 and S3). For both spectra, acetonitrile is the quintet at 1.96 ppm, and water is the singlet at 2.13 ppm. ^{13}C satellites are observable for the acetonitrile. In the blank spectrum (Fig. S2), residual acetone from cleaning the NMR tubes is seen at 2.11 ppm. For the blank, the amount of water by integration is 18% (i.e. the integrated value of water divided by the sum of integrated values). To determine the water content in the HPLC grade acetonitrile, the water peak integration was set to equal 0.24, which is seen in the blank. The amount of water in the solvent, then is <0.4%. This purity is sufficient for the variable-temperature experiments performed, and no adverse effects (e.g. bimodal Arrhenius behavior, unexpected room temperature lifetimes) are observed.
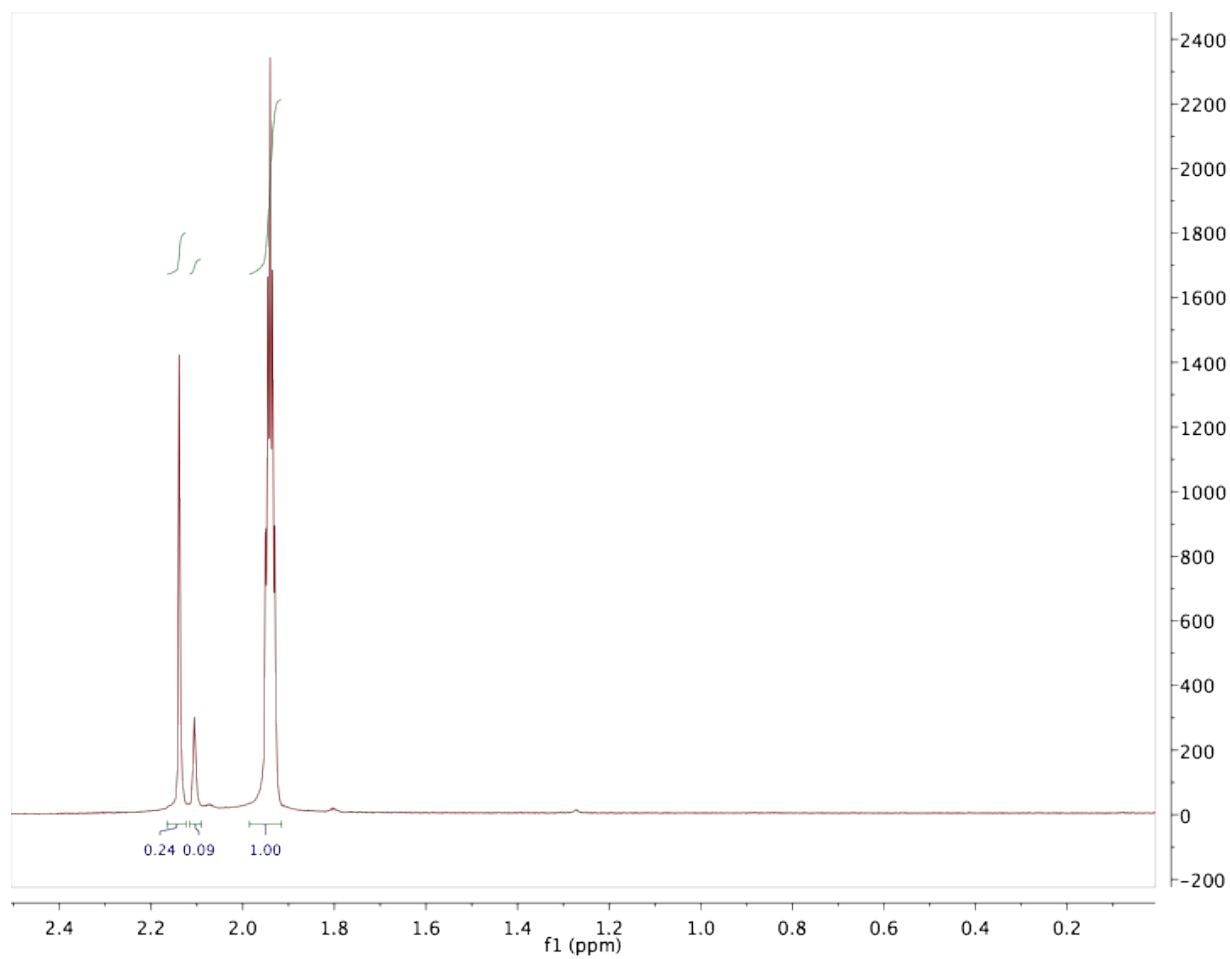
Figure S2. *^{1}H NMR of CD$_3$CN blank. Assignments can be found in the text.*
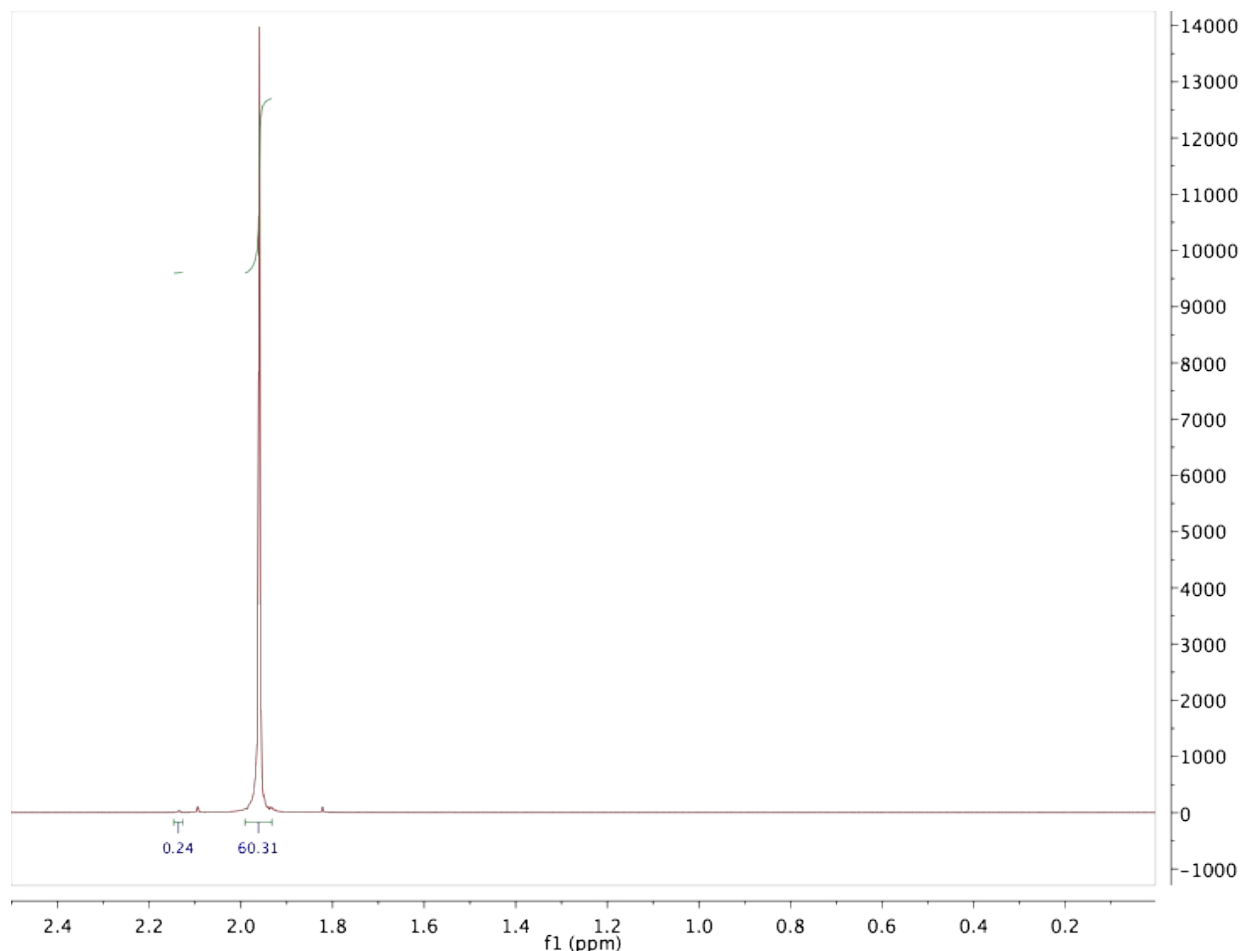
Figure S3.   *^{1}H NMR spectrum of spec-grade acetonitrile in CD[3]CN. Assignments can be found in the text.*

Effect of diethyl ether in lattice on lifetime of complexes. As previously mentioned, solvent can play a huge role in the lifetimes of Fe(II) polypyridyl complexes. The authors were concerned with the presence of diethyl ether in the ^{1}H NMR spectrum of $[Fe(dmb)_3]^{2+}$. On its face, this is hardly unusual as recrystallizations of these complexes are performed by diethyl ether diffusions into acetonitrile solutions.[2,3] Diethyl ether has also been observed in the crystal structures of some of the compounds, indicating its presence in the lattice.[3] However, by ^{1}H NMR, diethyl ether existed in a 1:2 mol ratio to $[Fe(dmb)_3]^{2+}$. As a solvent, its bulk properties are incredibly different from acetonitrile, which could be cause for concern. For example, the

dielectric constant of acetonitrile is 36.64, but is 4.27 in the case of diethyl ether.[4] Because the nature of the outer-sphere reorganization energy is unknown, the effect that the presence of ether will have on $^5T_2 \rightarrow {}^1A_1$ transition is also uncertain. To ensure that the variable-temperature results for $[Fe(dmb)_3]^{2+}$ were unchanged by the diethyl ether, a sample of $[Fe(bpy)_3](PF_6)_2$ was doped with excess diethyl ether (125 mol equiv.). The lifetime at room temperature was found to be 1030 ± 20 ps, which is identical to the undoped sample. However, there was the possibility that the ether could somehow affect the energetics of one electronic state more than the other, thereby changing the activation energy (E_a). Variable-temperature measurements were then made, and E_a was found to be 310 ± 15 cm^{-1} (Fig. 4 and 5). Due to the similarity in nature of $[Fe(bpy)_3]^{2+}$ and $[Fe(dmb)_3]^{2+}$, it can definitively be concluded that at this concentration, the diethyl ether does not significantly affect either the room temperature lifetime, or the Arrhenius parameters for these Fe(II) complexes.
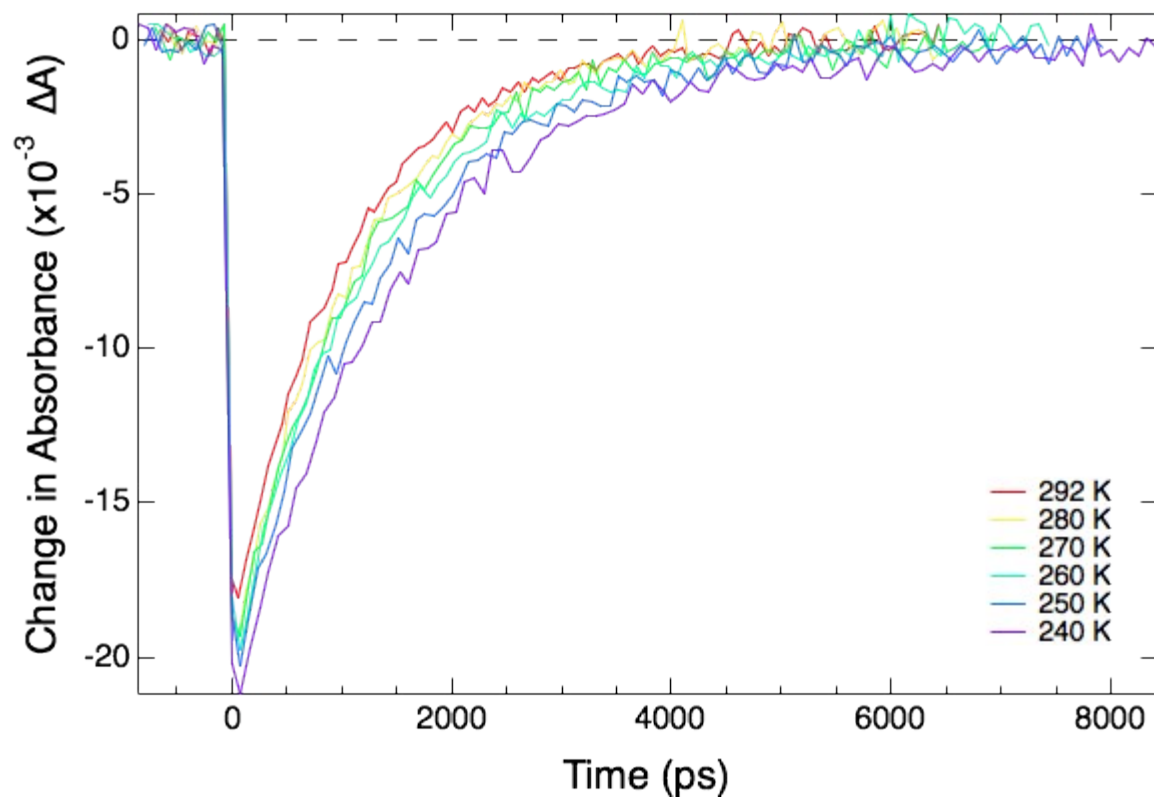
Figure S4. *Ground state recovery lifetimes of [Fe(bpy)₃]²⁺ doped with 125 mol equiv. of diethyl ether, as a function of temperature. Excitation was performed at 490 nm, and the probe was 530 nm. Lifetimes at the various temperatures are within error of those reported for the sample without diethyl ether.*
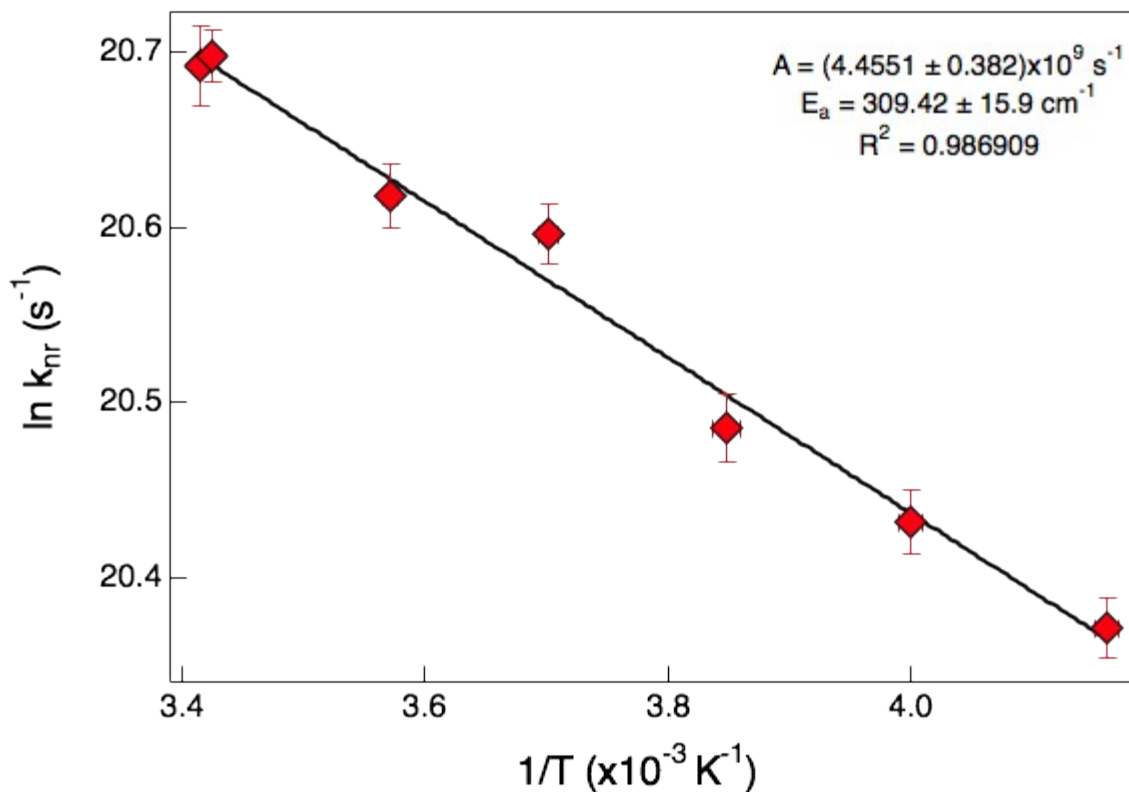
Figure S5. Arrhenius plot of the averaged variable-temperature data of [Fe(bpy)₃]²⁺ doped with 125 mol equiv. of diethyl ether. The preexponential factor, A, was found to be 225 ± 20 ps⁻¹, with the activation energy being 310 ± 15 cm⁻¹. These values are in excellent agreement with the Arrhenius factors found for the undoped [Fe(bpy)₃]²⁺ sample. The data fit well (R² = 0.99) to a single mode.

Variable-temperature ultrafast data.
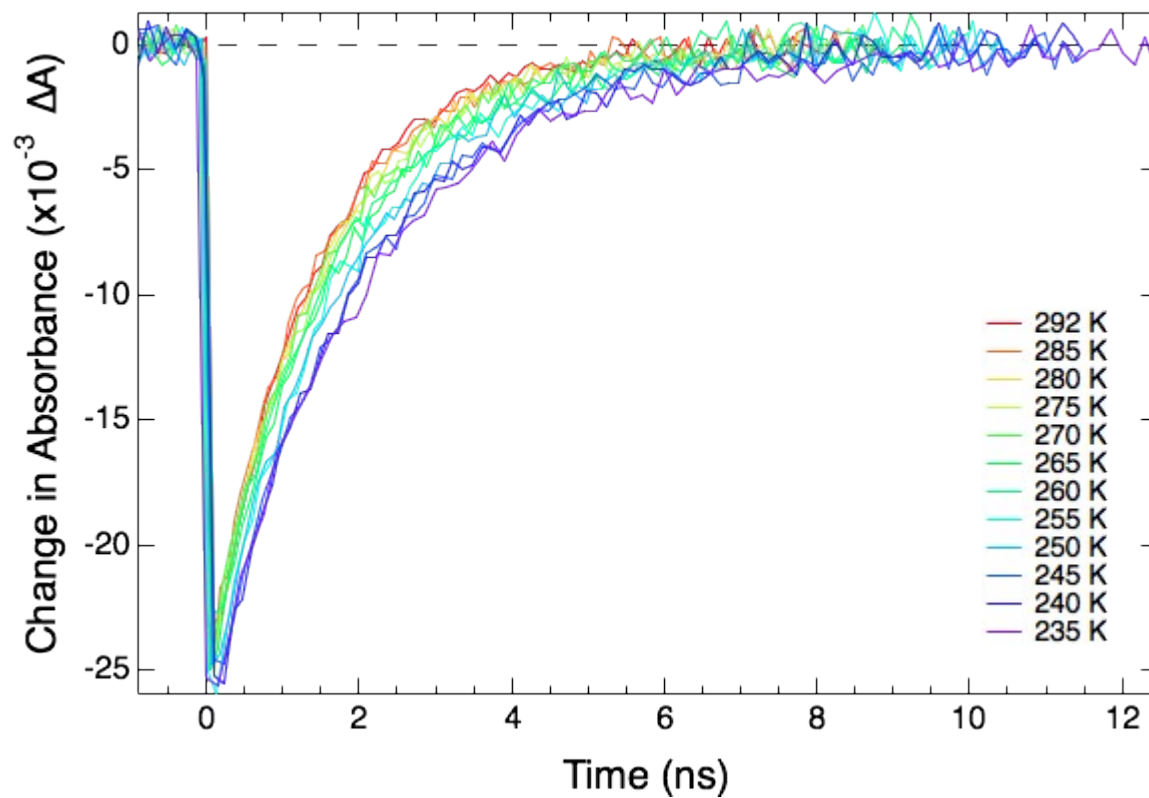
Figure S6. *Ground state recovery lifetimes of [Fe(dmb)₃]²⁺ as a function of temperature. Excitation was performed at 490 nm, and the probe was 530 nm.*
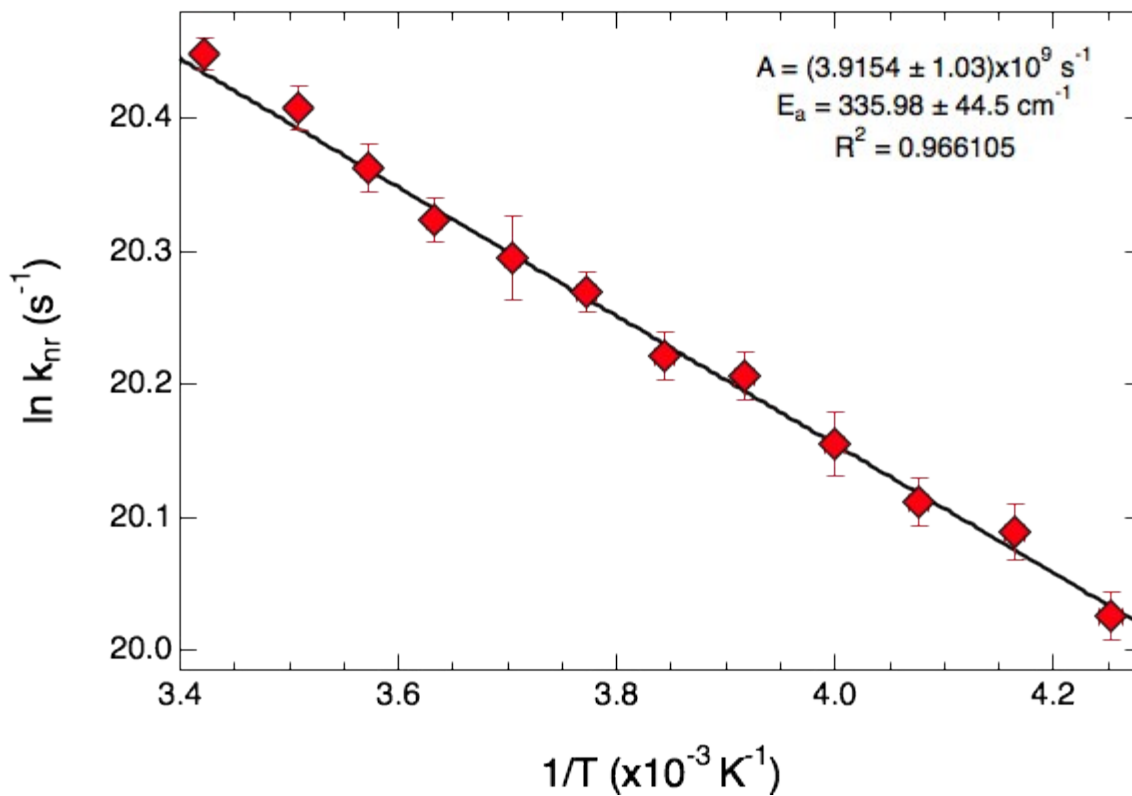
Figure S7. *Arrhenius plot of the averaged [Fe(dmb)₃]²⁺ variable-temperature data. The preexponential factor, A, was found to be 240 ± 20 ps⁻¹, with the activation energy being 345 ± 10 cm⁻¹. The data fit well (R² = 0.97) to a single mode.*
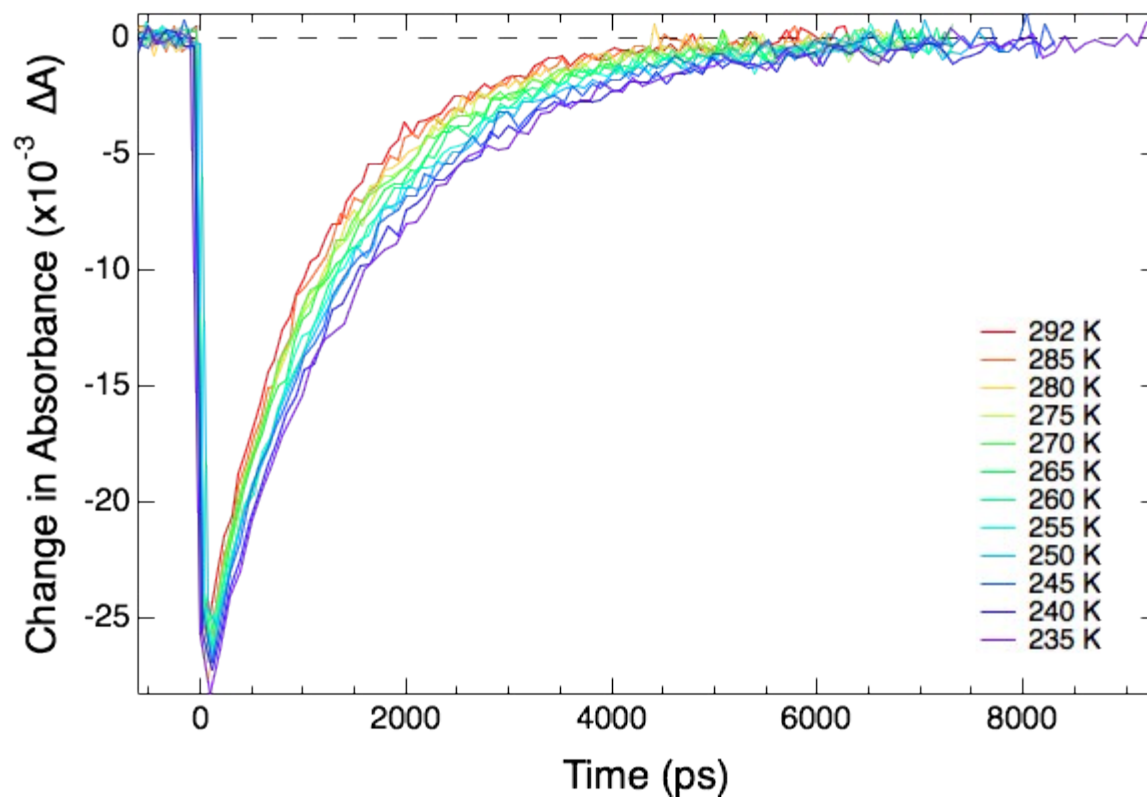
Figure S8. *Ground state recovery lifetimes of [Fe(dtbb)₃]²⁺ as a function of temperature. Excitation was performed at 490 nm, and the probe was 530 nm.*
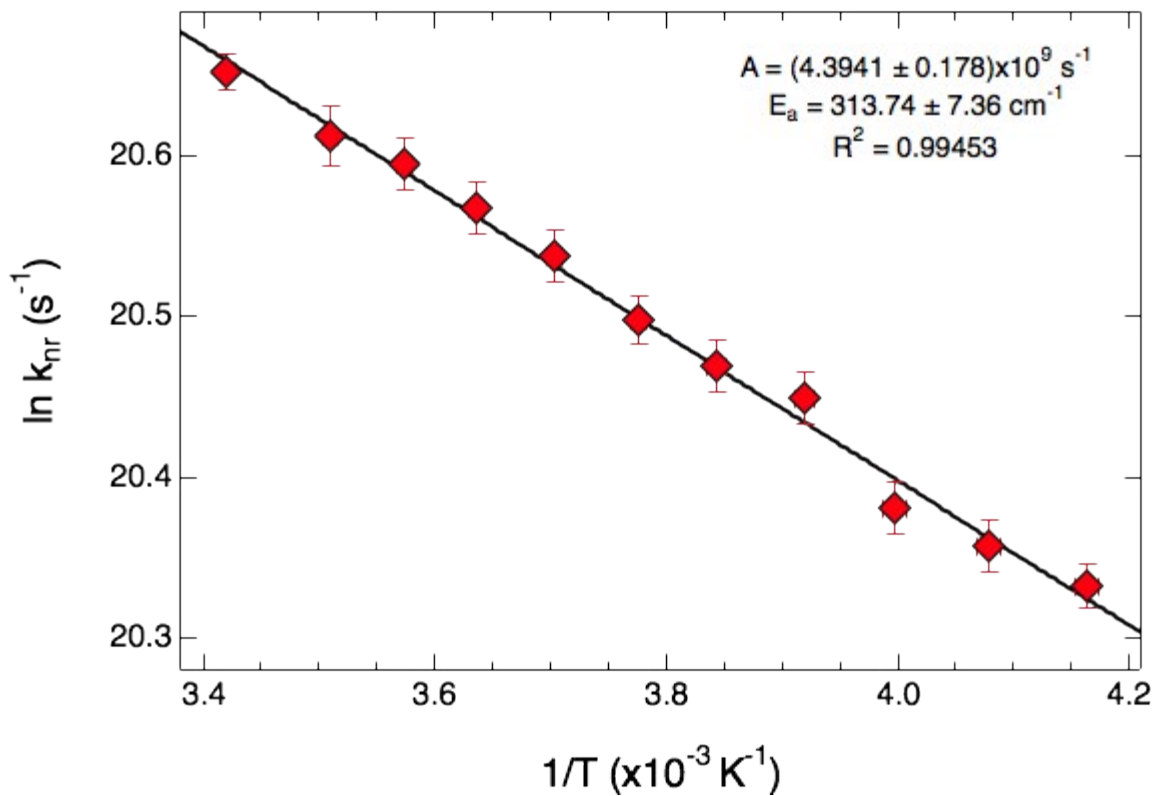
Figure S9. *Arrhenius plot of the averaged [Fe(dtbb)₃]²⁺ variable-temperature data. The preexponential factor, A, was found to be 230 ± 15 ps⁻¹, with the activation energy being 315 ± 15 cm⁻¹. The data fit well (R² = 0.99) to a single mode.*
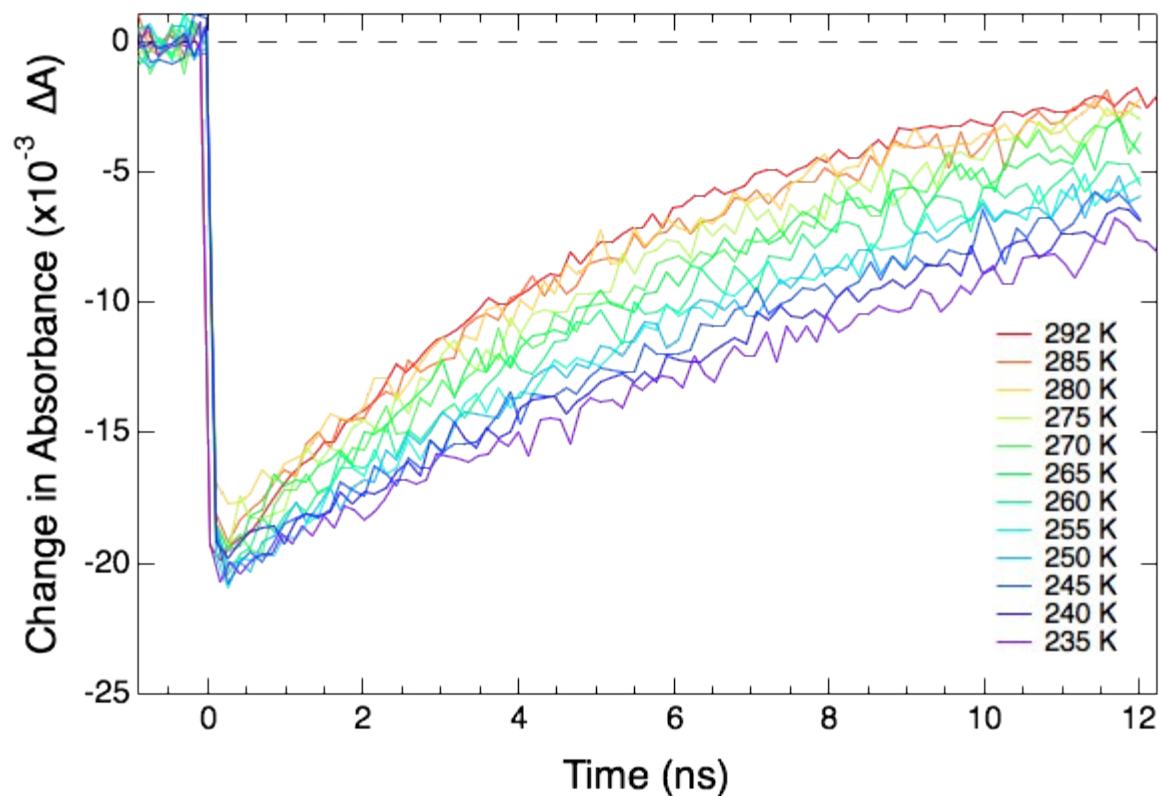
Figure S10. *Ground state recovery lifetimes of [Fe(terpy)₃]²⁺ as a function of temperature. Excitation was performed at 490 nm, and the probe was 530 nm. Because of the delay stage used in this experiment, at no temperature does the molecule recover the ground state fully (i.e. the signal returns to zero). This effect is only worsened at cold temperatures, to such an extent that the signal appears to be linear. These issues give rise to the increase in uncertainty on the lifetimes and subsequently calculated values.*
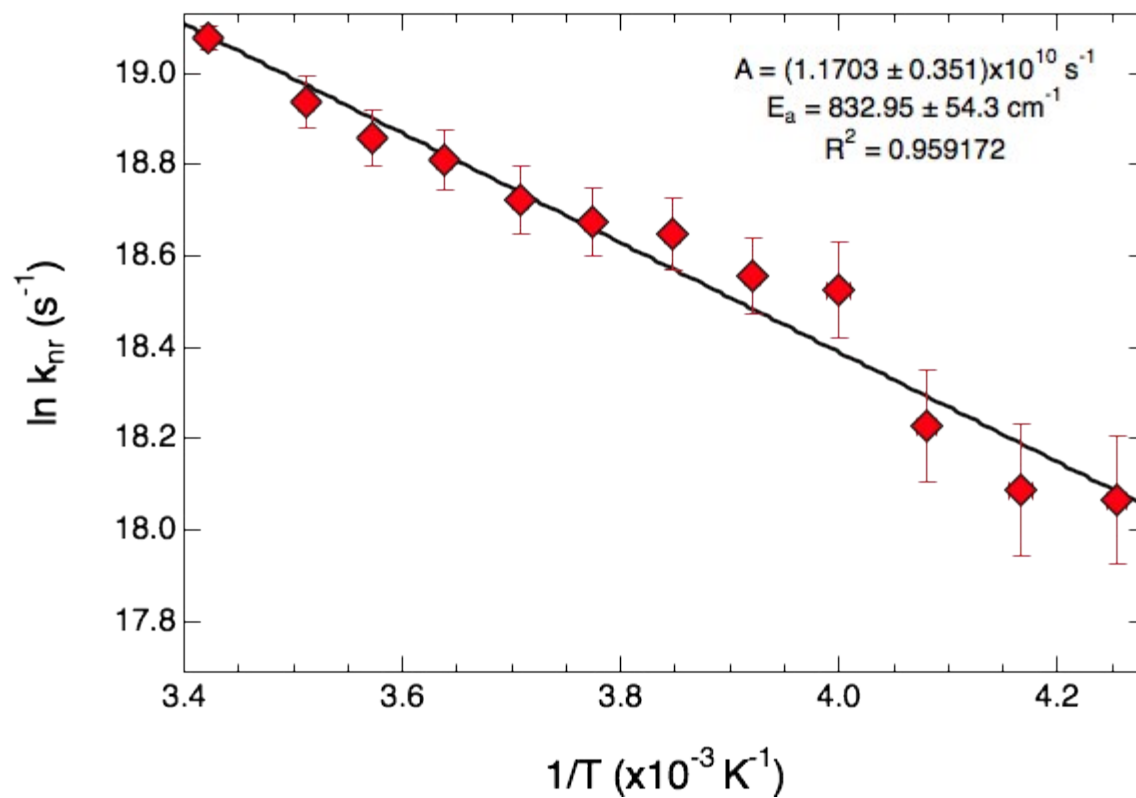
Figure S11. *Arrhenius plot of the averaged [Fe(terpy)$_2$]$^{2+}$ variable-temperature data. The preexponential factor, A, was found to be 150 ± 55 ps^{-1}, with the activation energy being 755 ± 70 cm^{-1}. The data fit well (R^2 = 0.96) to a single mode.*
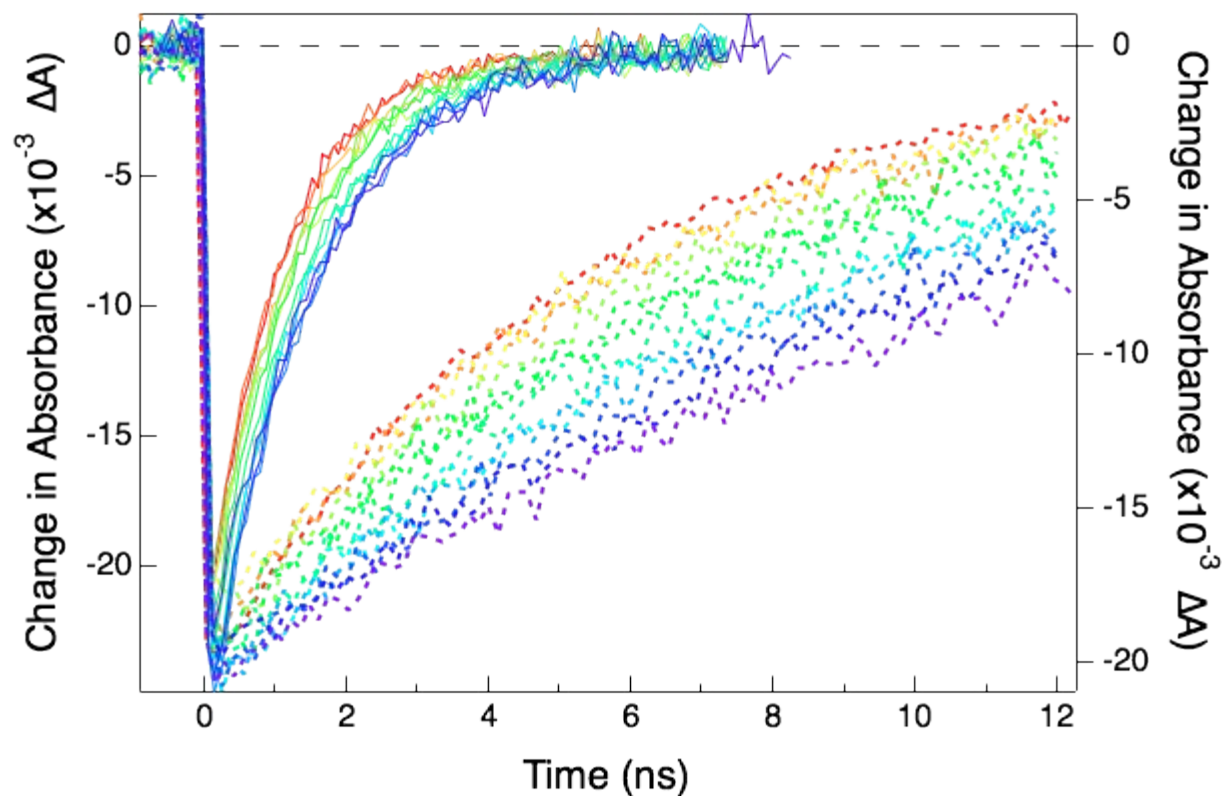
Figure S12. *Overlay of the variable-temperature ultrafast transient absorption spectra for [Fe(bpy)₃]²⁺ (—) and [Fe(terpy)₂]²⁺ (--). The traces indicate the temperature of the sample, red being 292 K to purple being 235 K. The left axis shows the scale for the [Fe(bpy)₃]²⁺, whereas [Fe(terpy)₂]²⁺ is plotted against the right axis.*
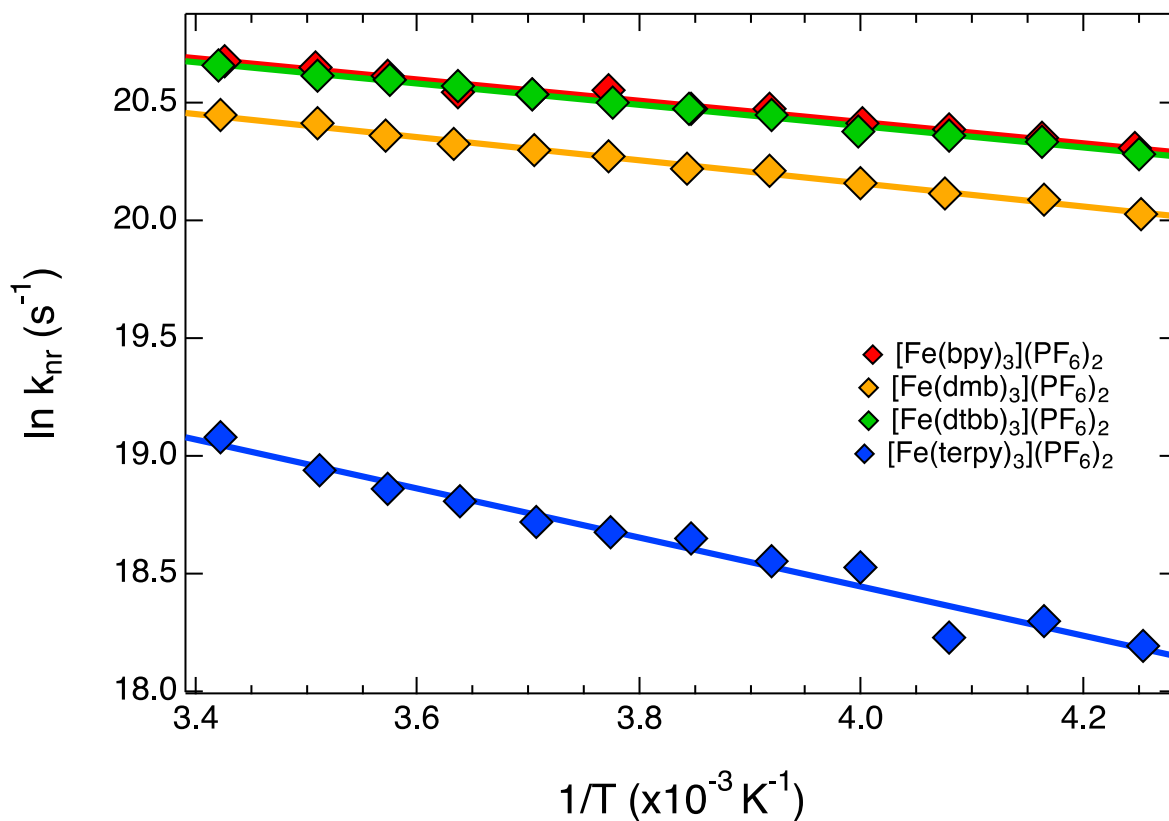
Figure S13. *Comparison of the Arrhenius plots for the four complexes. The data are displayed as diamonds, and the straight line is the fit of the data: [Fe(bpy)₃]²⁺ in red, [Fe(dmb)₃]²⁺ in orange, [Fe(dtbb)₃]²⁺ in green, and [Fe(terpy)₂]²⁺ in blue.*

Data Analysis

Based on the optical material, the exact amount of dispersion introduced to a pulse as it propagates through that material.[5] These calculations are defined by variables such as group velocity delay (GVD) and group delay dispersion (GDD), which is in turn determined by properties that are specific to the type of glass or material through which the pulse is traveling. For our purposes, the calculations were made for fused silica, the glass of the optical windows of the cryostat. There are four windows (two in the outer jacket, two in the inner jacket) plus the two glass faces of the sample cuvette, summing to approximately 12 mm of fused silica. Based on the material properties and this distance, the GVD can be found as a function of wavelength according to

$$GVD = \frac{\lambda^3}{2\pi c^2}\left(\frac{d^2n}{d\lambda^2}\right)$$

(S1)

In which λ is wavelength, c is the speed of light, and $(d^2n/d\lambda^2)$ is the second derivative of the index of refraction for the material. The GDD (φ_2) of the material is then the product of the GVD and the distance of material through which the pulse is propagating. Here, that distance is 12 mm. To determine the temporal effect that dispersion will have on a pulse of a certain input duration (Δt_{in}), Δt_{out} can be calculated from the GDD at a specific wavelength:

$$\Delta t_{out} = \frac{\sqrt{\Delta t_{in}^4 + 16(ln2)^2\varphi_2^2}}{\Delta t_{in}}$$

(S2)

The results of this calculation can be found in Fig. S14 comparing a pulse that travels through no media, and a pulse traveling through 12 mm of fused silica (i.e. the setup reported here). In general, as the amount of glass increases, the output pulse is lengthened more relative to the input pulse. This effect is especially dominant in pulses <40 fs. In the case of a 20 fs pulse, the output is broadened to 119 fs, six times the original pulse duration. For the setup used in this

work, however, the pulses were on the order of 150 fs, for which almost no broadening is calculated – or experimentally observed. These calculations serve to reinforce the idea that variable-temperature measurements are experimentally challenging on the ultrafast timescale for reasons such as pulse broadening.
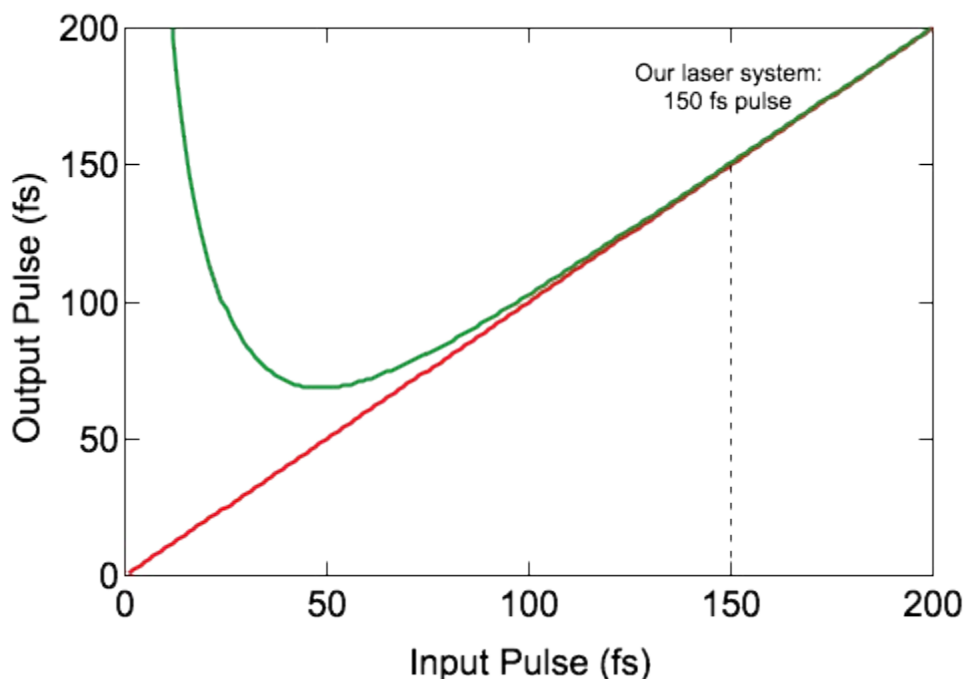
Figure S14. Calculated effects of group velocity delay (GVD) or dispersion on an ultrafast laser pulse. The red trace shows an input pulse that does not traverse through media, and is therefore equivalent to its output pulse. In green is the calculated duration of a pulse at 490 nm propagating through 12 mm of fused silica. The dashed line denotes 150 fs, which is the pulse duration used in the work reported here.

Error propagation. For the ground state recovery rates that were collected, each temperature trace that is reported is an average of approximately 10 scans. An in-house LabVIEW program processes the data and writes the average and standard deviation at each time delay. Additionally, the "average + standard deviation" and "average - standard deviation" are written. All three calculated averages are then fit with a single exponential in IgorPro. The time

constant reported is the tau calculated for the average. The error bars for a lifetime are given by the average error on the fit for the "average + standard deviation" and "average - standard deviation" data. This gives the most accurate representation of the error on the fits.

When a mathematical process is performed on a value that has error associated with it (e.g., the averaging of activation energies outlined below), the uncertainty must be propagated. There are many methods of propagating uncertainty available.[6] Some are meant for statistical analysis, requiring large population sizes of data, and are thus not well-suited for the work herein. Another problem with the methods readily found is that there is a tendency to over- or under-estimate the error. Through rigorous empirical testing, we have found that the best method for propagating uncertainty given the size of the data sets being worked with is to take the standard deviation of the extreme ends of each value. "Extreme ends" here refers to the average plus or minus the error. The averages themselves should not be considered for the standard deviation calculation, as they will serve to increase the size of the sample but not the error, and will therefore artificially decrease the magnitude of uncertainty. Error bars reported within this work use the method as outlined above.

Data were collected for each complex at each temperature at least twice. The Arrhenius parameters were checked in three different ways to determine self-consistency and the appropriate size of error. In the first method, each complete data set was worked up to determine the Arrhenius parameters for those data. All Arrhenius values for a given complex were averaged. Secondly, all the data were plotted as k_{nr} versus inverse temperature and A and E_a were calculated from the fit of the accumulated data. Finally, the average of all the data were plotted in an Arrhenius plot, and parameters were determined from the fit. In the case of the $[Fe(bpy')_3]^{2+}$ series, the averages of E_a were within 10 cm^{-1} of each other. For $[Fe(terpy)_3]^{2+}$, they

were within 35 cm^{-1} of each other. The same procedure was performed on A, and similar results were seen. These methods verify the robustness of the data collected.

Evaluation of Marcus parameters. In order to solve for Marcus parameters, relationships to the Arrhenius equation must be utilized. With an initial value of ΔG^o assumed from Table 2 (from the main text) and the value of A found from the Arrhenius plots, eq 2 (from the main text) is used to find the two values possible for λ due to the parabolic nature of the Marcus activation energy. For example, for $[Fe(bpy)_3]^{2+}$, $\Delta G^o = -7300 \pm 730$ cm^{-1} and $E_a = 310 \pm 15$ cm^{-1}. From these, $\lambda = 4850$ or 10980 cm^{-1}. $[Fe(bpy)_3]^{2+}$ is believed to be barrierless, and in this region, $-\Delta G^o < \lambda$,[7] therefore $\lambda = 11000$ cm^{-1}. To determine the size of the error bars on this value, the uncertainty of ΔG^o and E_a are propagated. For this, the "extreme ends" of each parameter are used in every combination to calculate λ, according to Table S2. Ultimately, it is found that $\lambda = 11000 \pm 1000$ cm^{-1}.

Table S2. Propagation of uncertainties in ΔG^o and E_a to calculate λ.

	ΔG^o (cm^{-1})	E_a (cm^{-1})	λ (cm^{-1})
Upper ΔG^o, Upper E_a	-6570	325	10200
Upper ΔG^o, Lower E_a	-6570	295	12000
Lower ΔG^o, Upper E_a	-8030	325	10000
Lower ΔG^o, Lower E_a	-8030	295	11700
Average	-7300 ± 730	310 ± 15	11000 ± 1000

Once a value of λ has been determined, eqn. 5 can be used to solve for H_{ab} analytically. This is also how H_{ab}^4/λ is calculated. To verify the values of H_{ab} that were found using this

method, A is used to calculate the H_{ab}^4/λ ratio for a variety of H_{ab} and λ values. Based on the error associated with A, a range of ratios is therefore known. This range is explored within the given range of λ values as determined above to find the appropriate H_{ab} average and its uncertainty. For example: the preexponential factor for $[Fe(bpy)_3]^{2+}$ is 230 ± 20 ps^{-1}. In solving for H_{ab}^4/λ, the range found using eqn. 5 is 0.0286-0.0412. Using this ratio and the reorganization energy gives $H_{ab} = 4.4 \pm 0.2$ cm^{-1}. From Table S1, λ is known to fall within 10000-12000 cm^{-1}. A table is made for $H_{ab} = 0$-10 cm^{-1} in steps of 0.1 cm^{-1} for $\lambda = 10000$-12000 cm^{-1}. The only values of H_{ab} that give a ratio within the window found from the experimentally determined value of A for $[Fe(bpy)_3]^{2+}$ are 4.1-4.7 cm^{-1}, or $H_{ab} = 4.4 \pm 0.3$ cm^{-1}. This range is in excellent agreement with the values found analytically.

References.

1. J. N. Miller and J. K. McCusker. *Manuscript in preparation*.

2. L. L. Jamula, A. M. Brown, D. Guo and J. K. McCusker, *Inorg. Chem.*, 2014, **53**, 15-17.

3. J. England, C. C. Scarborough, T. Weyhermüller, S. Sproules and K. Wieghardt, *Eur. J. Inorg. Chem.*, 2012, **2012**, 4605-4621.

4. CRC Handbook of Chemistry and Physics, 98th ed., http://hbcponline.com/faces/documents/06_33/06_33_0001.xhtml, (accessed September 2017).

5. Newport Application Note 29, http://assets.newport.com/webDocuments-EN/images/12243.PDF, (accessed November 2017).

6. I. Farrance and R. Frenkel, *Clin. Biochem. Rev.*, 2012, **33**, 49-75.

7. N. Sutin, *Acc. Chem. Res.*, 1982, **15**, 275-282.